Material thickness optimization for transmission-mode terahertz time-domain spectroscopy

Withawat Withayachumnankul [1,2], Bernd M. Fischer [1], and Derek Abbott [1]

[1] *School of Electrical & Electronic Engineering, The University of Adelaide, Adelaide, SA 5005, Australia*

[2] *Department of Information Engineering, Faculty of Engineering, King Mongkut's Institute of Technology Ladkrabang, Bangkok 10520, Thailand*

withawat@eleceng.adelaide.edu.au

http://www.eleceng.adelaide.edu.au/thz/

Abstract: The thickness of a sample material for a transmission-mode terahertz time-domain spectroscopy (THz-TDS) measurement is the subject of interest in this paper. A sample that is too thick or too thin can raise the problem of measurement uncertainty. Although greater thickness allows the terahertz radiation—or T-rays—to interact more with bulk material, the SNR rolls off with thickness due to signal attenuation. A sample that is too thin renders itself nearly invisible to T-rays, in such a way that the system can hardly sense the difference between the sample and a free space path. The optimal trade-off is analyzed and revealed in this paper, where our approach is to find the optimal thickness that results in the minimal uncertainty of measured optical constants. The derived model for optimal thickness is supported by the results from experiments performed with polyvinyl chloride (PVC), high-density polyethylene (HDPE), and lactose samples.

OCIS codes: (000.2170) Equipment and techniques; (120.4530) Optical constants; (080.1753) Computation methods; (300.1030) Absorption; (300.6495) Spectroscopy, terahertz

References and links

1. D. Abbott and X.-C. Zhang, "Scanning the issue: T-ray imaging, sensing, and retection," Proc. IEEE **95**, 1509–1513 (2007).
2. R. Huber, A. Brodschelm, F. Tauser, and A. Leitenstorfer, "Generation and field-resolved detection of femtosecond electromagnetic pulses tunable up to 41 THz," Appl. Phys. Lett. **76**, 3191–3193 (2000).
3. K. Liu, J. Xu, and X.-C. Zhang, "GaSe crystals for broadband terahertz wave detection," Appl. Phys. Lett. **85**, 863–865 (2004).
4. Z. Jiang and X.-C. Zhang, "Measurement of spatio-temporal terahertz field distribution by using chirped pulse technology," IEEE J. Quantum Electron. **36**, 1214–1222 (2000).
5. A. Bartels, A. Thoma, C. Janke, T. Dekorsy, A. Dreyhaupt, S. Winnerl, and M. Helm, "High-resolution THz spectrometer with kHz scan rates," Opt. Express **14**, 430–437 (2006). URL http://www.opticsexpress.org/abstract.cfm?URI=oe-14-1-430.
6. T. Yasui, E. Saneyoshi, and T. Araki, "Asynchronous optical sampling terahertz time-domain spectroscopy for ultrahigh spectral resolution and rapid data acquisition," Appl. Phys. Lett. **87**, 061101 (2005).

#94045 - $15.00 USD Received 20 Mar 2008; revised 30 Apr 2008; accepted 1 May 2008; published 6 May 2008

7. R. H. Jacobsen, D. M. Mittleman, and M. C. Nuss, "Chemical recognition of gases and gas mixtures with terahertz waves," Opt. Lett. **21**, 2011–2013 (1996).
8. C. J. Strachan, P. F. Taday, D. A. Newnham, K. C. Gordon, J. A. Zeitler, M. Pepper, and T. Rades, "Using terahertz pulsed spectroscopy to quantify pharmaceutical polymorphism and crystallinity," J. Pharm. Sci. **94**, 837–846 (2005).
9. S. Gorenflo, U. Tauer, I. Hinkov, A. Lambrecht, R. Buchner, and H. Helm, "Dielectric properties of oil–water complexes using terahertz transmission spectroscopy," Chem. Phys. Lett. **421**, 494–498 (2006).
10. M. van Exter, C. Fattinger, and D. Grischkowsky, "Terahertz time-domain spectroscopy of water vapor," Opt. Lett. **14**, 1128–1130 (1989).
11. W. Withayachumnankul, G. M. Png, X. X. Yin, S. Atakaramians, I. Jones, H. Lin, B. S. Y. Ung, J. Balakrishnan, B. W.-H. Ng, B. Ferguson, S. P. Mickan, B. M. Fischer, and D. Abbott, "T-ray sensing and imaging," Proc. IEEE **95**, 1528–1558 (2007).
12. M. van Exter and D. Grischkowsky, "Characterization of an optoelectronic terahertz beam system," IEEE Trans. Microw. Theory Tech. **38**, 1684–1691 (1990).
13. A. Poppe, L. Xu, F. Krausz, and C. Spielmann, "Noise characterization of sub-10-fs Ti:sapphire oscillators," IEEE J. Sel. Top. Quantum Electron. **4**, 179–184 (1998).
14. N. Cohen, J. W. Handley, R. D. Boyle, S. L. Braunstein, and E. Berry, "Experimental signature of registration noise in pulsed terahertz systems," Fluct. Noise Lett. **6**, L77–L84 (2006).
15. D. M. Mittleman, R. H. Jacobsen, and M. C. Nuss, "T-ray imaging," IEEE J. Sel. Top. Quantum Electron. **2**, 679–692 (1996).
16. P. U. Jepsen and B. M. Fischer, "Dynamic range in terahertz time-domain transmission and reflection spectroscopy," Opt. Lett. **30**, 29–31 (2005).
17. W. Feller, "The fundamental limit theorems in probability," Bull. Amer. Math. Soc. **51**, 800–832 (1945).
18. H. F. Trotter, "An elementary proof of the central limit theorem," Arch. Math. **10**, 226–234 (1959).
19. W. Withayachumnankul, B. M. Fischer, H. Lin, and D. Abbott, "Uncertainty in terahertz time-domain spectroscopy measurement," J. Opt. Soc. Am. B (2008). (In press).
20. L. Thrane, R. H. Jacobsen, P. U. Jepsen, and S. R. Keiding, "THz reflection spectroscopy of liquid water," Chem. Phys. Lett. **240**, 330–333 (1995).
21. B. M. Fischer, "Broadband THz time-domain spectroscopy of biomolecules – A comprehensive study of the dielectric properties of biomaterials in the far-infrared," Ph.D. thesis, Department of Molecular and Optical Physics, Freiburg Materials Research Center, Universität Freiburg (2005).
22. Y.-S. Jin, G.-J. Kim, and S.-G. Jeon, "Terahertz dielectric properties of polymers," J Korean Phys. Soc. **49**, 513–517 (2006).
23. S. P. Mickan, R. Shvartsman, J. Munch, X. C. Zhang, and D. Abbott, "Low noise laser-based T-ray spectroscopy of liquids using double-modulated differential time-domain spectroscopy," J Opt. B-Quantum S. O. **6**, S786–S795 (2004).
24. R. Piesiewicz, C. Jansen, S. Wietzke, D. Mittleman, M. Koch, and T. Kürner, "Properties of building and plastic materials in the THz range," Int. J Infrared Milli. **28**, 363–371 (2007).
25. B. M. Fischer, M. Hoffmann, and H. Helm, G. Modjesch, P. U. Jepsen, "Chemical recognition in terahertz time-domain spectroscopy and imaging," Semicond. Sci. Technol. **20**, S246–S253 (2005).
26. A. G. Markelz, "Terahertz dielectric sensitivity to biomolecular structure and function," IEEE J. Sel. Top. Quantum Electron. **14**, 180–190 (2008).
27. L. Duvillaret, F. Garet, and J.-L. Coutaz, "A reliable method for extraction of material parameters in terahertz time-domain spectroscopy," IEEE J. Sel. Top. Quantum Electron. **2**, 739–746 (1996).
28. L. Duvillaret, F. Garet, and J.-L. Coutaz, "Highly precise determination of optical constants and sample thickness in terahertz time-domain spectroscopy," Appl. Opt. **38**, 409–415 (1999).

1. Introduction

Teraherz time-domain spectroscopy (THz-TDS) is a promising tool of determining the complex response of materials at T-ray frequencies, bounded between 0.1 and 10 THz [1]. In a transmission measurement, the system generates and detects coherent broadband pulses, which, once transmitted through a sample, have their shape changed in accordance with the sample's frequency response. This enables estimation of optical constants, or related quantities, of the sample from the measured pulses. Recent developments for the system mainly aim for wider bandwidth [2, 3] and faster scan rates [4, 5, 6]. Another important aspect that needs consideration is the uncertainty in the extracted optical constants.

The uncertainty in the optical constants is deemed crucial in many THz-TDS applications. Some applications that require a remarkably low uncertainty in measurement include quantify-

#94045 - $15.00 USD Received 20 Mar 2008; revised 30 Apr 2008; accepted 1 May 2008; published 6 May 2008

ing the sample amount [7, 8, 9], determining resonance frequencies [10], etc. In certain cases, a lower uncertainty assists the interpretation of data at a critical point. An example is when a small resonance is overwhelmed by noise, resulting in an ambiguous observation. A lower uncertainty in measurement could resolve the issue.

A major contribution to the uncertainty in the measured optical constants is from the fluctuations and noise in the measured signals [11], which are mainly due to electronic [12], optical [13], and mechanical [14] components. Thus, in order to reduce the uncertainty in optical constants, one may attempt to tackle the noise in the signals directly. It is known that using a lock-in amplifier with optical chopper to modulate T-ray signals [15] can reduce $1/f$ noise due to laser fluctuations. Also increasing the signal strength in the first place helps to lessen the effect of electrical and optical noise sources, by increasing the SNR. However, both of these approaches cannot solve the problem of mechanical drift. Alternatively, multiple scans are taken so that repeated measurements can be averaged in an attempt to reduce noise—however, this does not work if mechanical drift manifests between successive scans. A further approach to reduction of the uncertainty in optical constants is hidden in the details of sample geometry and its optimization—for the first time we now analyze this case and back up our theory with experimental results in this paper.

It is well known to every THz-TDS experimentalist that, in transmission-mode spectroscopy, a sample that is too thick has considerable bulk absorption and can significantly reduce the signal power. In fact, the upper bound of the thickness for a given absorption value is determined from the system's dynamic range [16]. Therefore, a sample is usually made very thin as long as it can be mechanically supported. However, a sample that is too thin can also cause problems, as the system might not be sufficiently sensitive to detect the resultant changes in the amplitude and phase of the signal. Both thickness extremes result in higher uncertainty in the measured optical constants. In this paper, the optimal trade-off between the two extremes is determined, in order to minimize the uncertainty in optical constants.

This paper is organized as follows: In Section 2, an analytical model relating the variance in signals to the variance in optical constants is introduced. This model leads to the optimization of the sample thickness based on minimization of the variance in optical constants, as shown in Section 3. An analytical formula for optimum thickness is verified by THz-TDS experiments with various materials in Section 4. The usage of the formula is discussed in Section 5.

2. Uncertainty in optical constants

The amplitude of T-ray signals is prone to noise induced by many sources. These sources include laser intensity fluctuations, optical and electronic noise, jitter in the delay stage, alignment error, mechanical drift, etc. Whilst most of the sources of error obey a normal distribution, alignment error and mechanical drift do not. However, via the Central Limit Theorem [17, 18], we might expect the resultant of all the errors tends towards a normal distribution. Hence, considered here is an amplitude variance model, which unifies all these errors and assumes a normal probability distribution. The influence of this amplitude variance on the uncertainty in extracted optical constants is shown in this section.

Given that the sample under a transmission-mode measurement has parallel and polished surfaces, and the angle of incidence of the incoming T-ray beam is normal to the surfaces, the transfer function of the sample is expressed as

$$H(\omega)=\frac{E_{\mathrm{sam}}(\omega)}{E_{\mathrm{ref}}(\omega)}=\tau\tau'\cdot\exp\left\{-\kappa(\omega)\frac{\omega l}{c}\right\}\cdot\exp\left\{-j[n(\omega)-n_0]\frac{\omega l}{c}\right\}, \tag{1}$$

where $E_{\mathrm{ref}}(\omega)$ and $E_{\mathrm{sam}}(\omega)$ are the reference and sample signals in the frequency domain, l is the sample thickness, $n(\omega)$ and $\kappa(\omega)$ are the refractive index and the extinction coefficient of

#94045 - $15.00 USD Received 20 Mar 2008; revised 30 Apr 2008; accepted 1 May 2008; published 6 May 2008

the sample, n_0 is the refractive index of air, and τ and τ' are the transmission coefficients at the sample interfaces. The refractive index and the extinction coefficient can be deduced from Eq. (1) as

$$n(\omega) = n_0 - \frac{c}{\omega l}\angle H(\omega)\,, \tag{2a}$$

$$\kappa(\omega) = \frac{c}{\omega l}\left\{\ln|\tau\tau'| - \ln|H(\omega)|\right\}\,. \tag{2b}$$

Influenced by the variance in measured signals, the variances in refractive index, $s_n^2(\omega)$, and in extinction coefficient, $s_\kappa^2(\omega)$, can be derived from Eq. (2) using the law of propagation of uncertainty. In brief, from the signal amplitudes in the time domain, the variance is transferred to the variance of the magnitude and phase spectra in the frequency domain via Fourier transform, as shown in [19]. Then the combination between the variances of sample and reference measurements produces the variance in the transfer function of a sample. The variance eventually appears at the optical constants. From this analysis, the variances in the refractive index and in the extinction coefficient are given by, respectively,

$$s_n^2(\omega) = \left(\frac{c}{\omega l}\right)^2\left\{\frac{A_{\rm sam}(\omega)}{|E_{\rm sam}(\omega)|^4} + \frac{A_{\rm ref}(\omega)}{|E_{\rm ref}(\omega)|^4}\right\}\,, \tag{3a}$$

$$s_\kappa^2(\omega) = \left(\frac{c}{\omega l}\right)^2\left\{\frac{B_{\rm sam}(\omega)}{|E_{\rm sam}(\omega)|^4} + \frac{B_{\rm ref}(\omega)}{|E_{\rm ref}(\omega)|^4} + \left(\frac{n(\omega)-n_0}{n(\omega)+n_0}\right)^2\frac{s_n^2(\omega)}{n(\omega)^2}\right\}\,, \tag{3b}$$

where

$$A_{\rm sam}(\omega) = \sum_k \Im^2[E_{\rm sam}(\omega)\exp(j\omega k\Delta)]s_{E_{\rm sam}}^2(k)\,, \tag{4a}$$

$$A_{\rm ref}(\omega) = \sum_k \Im^2[E_{\rm ref}(\omega)\exp(j\omega k\Delta)]s_{E_{\rm ref}}^2(k)\,, \tag{4b}$$

$$B_{\rm sam}(\omega) = \sum_k \Re^2[E_{\rm sam}(\omega)\exp(j\omega k\Delta)]s_{E_{\rm sam}}^2(k)\,, \tag{4c}$$

$$B_{\rm ref}(\omega) = \sum_k \Re^2[E_{\rm ref}(\omega)\exp(j\omega k\Delta)]s_{E_{\rm ref}}^2(k)\,. \tag{4d}$$

Here, $s_{E_{\rm ref}}^2(k)$ and $s_{E_{\rm sam}}^2(k)$ are the variances associated with the reference and sample signals, respectively; k is the sampling index number and Δ is the sampling interval, and thus $k\Delta$ is the time; $\Re^2$ and $\Im^2$ denote the square of real and imaginary parts, respectively. The summation is carried out over the time duration of the recorded T-ray signal. In the equations, all parameters utilize mean values. The proposed model in Eq. (3) is successfully validated using a Monte Carlo method [19]. The complete derivation for Eq. (3) can be found in [19].

3. Optimisation of the sample thickness

From Eq. (3a) and (3b) in Section 2, it can be inferred that four major variables, $n(\omega)$, $\kappa(\omega)$, l, and $|E_{\rm ref}|$, govern the amplitude-related variance, s_n^2 or s_κ^2. Optimising one of these parameters might help reduce the variance. Two of them, $n(\omega)$ and $\kappa(\omega)$, are intrinsic to materials, and thus cannot be optimized. The signal strength, $|E_{\rm ref}|$, without doubt, must be as large as possible—provided there is no damage to the sample—in order to minimize the variance. The sample thickness, l, can usually be controlled and thus may lend itself to optimization.

The intricate relation between the sample thickness and the standard deviation in the refractive index, s_n, is simulated and demonstrated via a contour plot in Fig. 1. As we can see, at

#94045 - $15.00 USD Received 20 Mar 2008; revised 30 Apr 2008; accepted 1 May 2008; published 6 May 2008

every frequency, there is an optimum sample thickness that gives the lowest s_n. Figure 2 reveals the magnitude of s_n and s_κ as a function of the thickness, estimated at three different example frequencies. The optimum thicknesses for the simulated sample at these frequencies approximately span from 300 μm to 1 mm. Moving towards a thicker sample by an order of magnitude sees an increment of the standard deviation by three orders. Moreover, moving towards a thinner sample by an order of magnitude results in increased standard deviation by one order of magnitude. Selecting the sample thickness to correspond to desired minimum in Fig. 2 is therefore advantageous.

According to the transfer function in Eq. (1),

$$|E_{\mathrm{sam}}(\omega)|^4 \quad = \quad (\tau\tau')^4 \exp\left\{-4\kappa(\omega)\frac{\omega l}{c}\right\} |E_{\mathrm{ref}}(\omega)|^4 \,. \tag{5}$$

Substituting Eq. (5) into Eq. (3a) and reassigning the notation gives

$$s_n^2(\omega) \quad = \quad \frac{C}{l^2}\left\{\frac{A'_{\mathrm{sam}}(\omega)}{\exp(-4\kappa\omega l/c)} + A_{\mathrm{ref}}(\omega)\right\} \,, \tag{6}$$

where

$$C = \frac{c^2}{\omega^2|E_{\mathrm{ref}}(\omega)|^4} \qquad \text{and} \qquad A'_{\mathrm{sam}}(\omega) = \frac{A_{\mathrm{sam}}(\omega)}{(\tau\tau')^4} \,. \tag{7}$$

Assuming that s_E^2 in $A(\omega)$ is not a function of l, we are now able to minimise $s_n^2(\omega)$ with respect to the thickness l. By taking the derivative of Eq. (6) with respect to l, we arrive at

$$\frac{\partial s_n^2(\omega)}{\partial l} \quad = \quad \left(4\frac{C}{l^2}\frac{\kappa\omega}{c} - 2\frac{C}{l^3}\right)\frac{A'_{\mathrm{sam}}(\omega)}{\exp(-4\kappa\omega l/c)} - 2\frac{C}{l^3}A_{\mathrm{ref}}(\omega) \,. \tag{8}$$

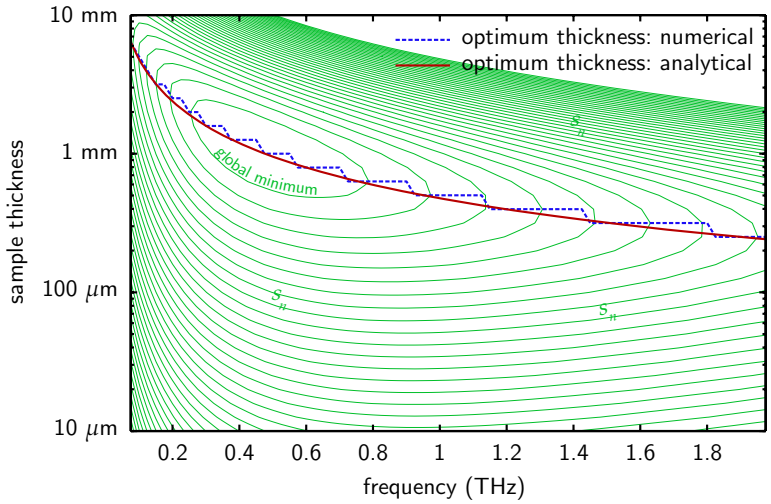

Fig. 1. Standard deviation in the refractive index against the sample thickness and frequency. The contours represent the simulated magnitude of s_n, which is in fact comparable to that of s_κ. The optical constants are set to $n - j\kappa = 3.0 - 0.1j$ at all frequencies ($\kappa = 0.1$ equals $\alpha = 41.9$ cm^{-1} at 1 THz). Additive white Gaussian noise limits the maximum dynamic range of the reference spectrum to 40 dB. The position of the global minimum relative to the frequency corresponds to the peak position of the reference spectrum. The profile of the optimum thickness determined numerically appears jagged due to the discrete nature of the simulation.

#94045 - $15.00 USD Received 20 Mar 2008; revised 30 Apr 2008; accepted 1 May 2008; published 6 May 2008

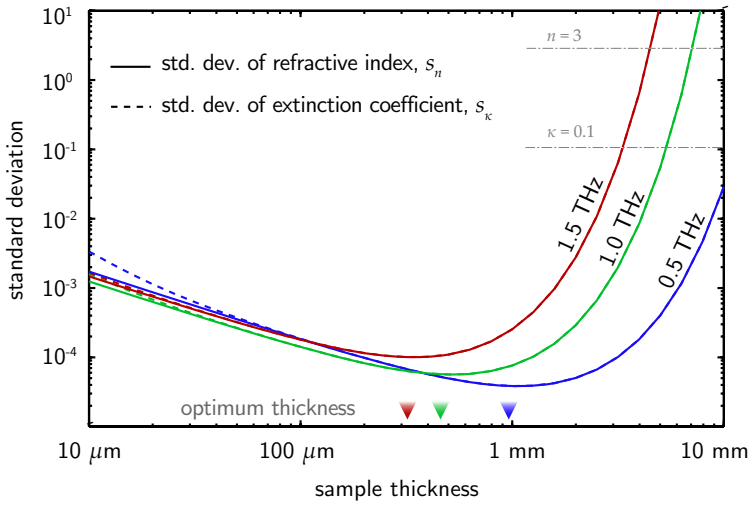

Fig. 2. Standard deviation in the optical constants against the sample thickness. The plots are cross-sectional profiles of Fig. 1, at selected frequencies 0.5, 1.0, and 1.5 THz. The optimum thicknesses, where the standard deviation is minimal, are indicated by arrowheads. By moving towards a thicker sample, the standard deviation rapidly increases to the point comparable to the optical constants' values. The standard deviation at high frequency is more sensitive to the thickness increment, as the T-ray magnitude at high frequencies is relatively low.

The variances in the reference and sample spectra, $A_{\mathrm{ref}}(\omega)$ and $A_{\mathrm{sam}}(\omega)$, can be related via the transfer function, as does the magnitude of the spectra in Eq. (5),

$$A_{\mathrm{sam}}(\omega) \quad \approx \quad (\tau\tau')^4 \exp\left\{-4\kappa(\omega)\frac{\omega l}{c}\right\} A_{\mathrm{ref}}(\omega)\,. \tag{9}$$

Note that the dependency of $A_{\mathrm{sam}}(\omega)$ on the sample thickness is an approximation, and does not affect the optimisation. Substituting Eq. (9) into Eq. (8) and equating to zero gives,

$$\left(4\frac{C}{l^2}\frac{\kappa\omega}{c} - 2\frac{C}{l^3}\right) A_{\mathrm{ref}}(\omega) - 2\frac{C}{l^3}A_{\mathrm{ref}}(\omega) \quad = \quad 0\,, \tag{10}$$

and further manipulation yields the optimum thickness:

$$l_{\mathrm{opt}} = \frac{c}{\omega\kappa(\omega)} = \frac{2}{\alpha(\omega)}\,. \tag{11}$$

The resultant optimum thickness obtained using Equation 11 is in accordance with the result obtained numerically, as demonstrated in Fig. 1.

By substituting the optimum thickness in Equation 11 into Equation 5 and ignoring reflection at the interfaces, we see that a sample with optimum thickness attenuates the magnitude of the incident pulse by the factor of $1/e$. The optimum thickness turns out to be a distance that is equal to twice the penetration depth. Optimization of the sample thickness by starting from Eq. (3b) also delivers the same outcome. Notice that the optimum thickness, l_{opt}, relies on neither the index of refraction, $n(\omega)$, nor the signal magnitude, $|E(\omega)|$. This is because the transmittance at the sample interfaces is not a function of thickness. In addition, the sensitivity of the detector

#94045 - $15.00 USD Received 20 Mar 2008; revised 30 Apr 2008; accepted 1 May 2008; published 6 May 2008

Table 1. Optimum sample thickness for some common materials determined by the proposed method. The optimum thickness for THz-TDS measurement is determined using Eq. (11). The absorption coefficients, measured at room temperature, are taken from various sources: water [20]; PMMA, TPX [21]; HDPE [22]. Note that the absorption coefficient can widely vary from sample to sample, in particular for plastics.

Material	0.5 THz		1.0 THz		1.5 THz	
	α (cm^{-1})	l_{opt}	α (cm^{-1})	l_{opt}	α (cm^{-1})	l_{opt}
Water	150	130 μm	200	100 μm	-	-
PMMA	5	4 mm	20	1 mm	40	0.5 mm
HDPE	2.0	10 mm	2.2	9.1 mm	2.4	8.3 mm
TPX	0.1	20 cm	0.5	4 cm	0.8	2.5 cm

is not involved, as the analysis aims for minimization of the uncertainty, i.e. stability of the measurement, for a given sensitivity.

In Table 1, some common dielectric materials with their optimal thicknesses are given, according to Eq. (11). In addition, it appears that the resultant thickness calculated from this equation is in close agreement with the result found numerically in [23], in which the optimization is for a differential thickness THz-TDS measurement. For example, at 1 THz, the optimum thickness for dioxane, which has $\kappa = 0.013$ or $\alpha = 5.45$ cm^{-1}, is reported to be 4 mm, and the optimum thickness for water, $\kappa = 0.478$ or $\alpha = 200$ cm^{-1}, is 100 μm [23]. Using the same parameters, the derived analytical expression given in Eq. (11) estimates the thicknesses for dioxane and water to be 3.7 mm and 100 μm, respectively.

4. Experiments and results

The experiments are performed using a fiber-coupled T-ray Picometrix 2000 system, equipped with photoconductive antennas for T-ray generation and detection. The pumping laser is a mode-locked Ti:Sa laser (MaiTai, Newport) with a central wavelength of 800 nm, a pulse duration of $<$80 fs, and a repetition rate of 80 MHz. The system generates pulsed T-ray radiation spanning from 0.05 to 1.5 THz, with a maximum dynamic range of 30 dB. The collimated beam diameter is approximately 25.4 mm. The sample materials that are used in this study are PVC, HDPE, and polycrystalline lactose, which have unique absorption characteristics. The reference measurement is made with a free path in two runs, ten scans each, before and after every run of ten individual sample measurements. The similarity of the variances of the two runs confirms no significant change to the hardware during sample measurement.

4.1. Polyvinyl chloride: PVC

The measurement is carried out with normal-grade PVC, which is preformed in a rod shape. The rod with a diameter of 50 mm is cut into four cylindrical segments, with the thickness of 1 (0.967), 10 (9.977), 20 (19.869), and 50 (50.338) mm—the values in parentheses are the average of five measurements with one standard deviation of $\approx \pm 0.005$ mm. The surfaces of these samples are well polished to minimize scattering. Each sample is measured with a collimated beam from the THz-TDS system in the axial direction for ten scans, and each scan is made after the previous scan within 30 sec.

The optical constants of PVC are extracted from the measurements of the 10-mm sample. The phase at low frequencies is extrapolated from the phase value between 0.05 and 0.1 THz. Figure 3 shows the extracted optical constants. Clearly, the refractive index is nearly constant

#94045 - $15.00 USD Received 20 Mar 2008; revised 30 Apr 2008; accepted 1 May 2008; published 6 May 2008

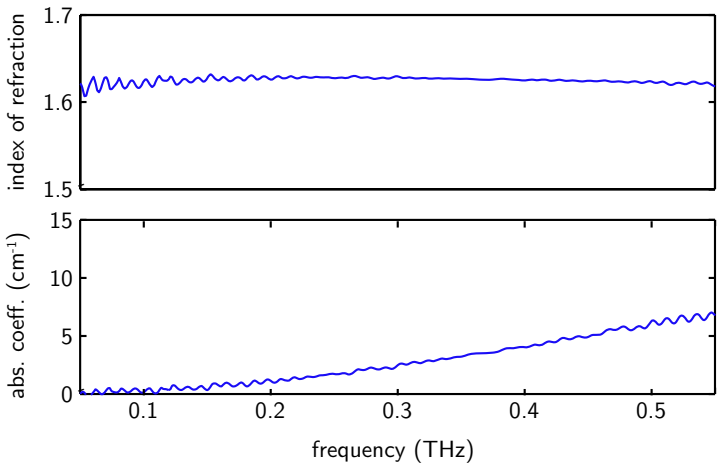

Fig. 3. Optical constants of PVC. The constants are calculated from the average signal probing a 10-mm-thick sample. The available bandwidth of the measurement is from 0.05 to 0.55 THz. The ripples in the curves are due to Fabry-Pérot reflections.

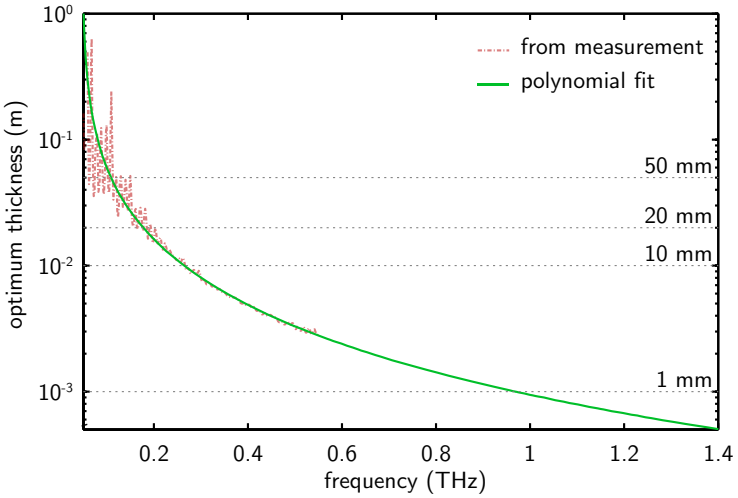

Fig. 4. Optimum thickness for PVC. The optimum thickness is determined from the measured absorption coefficient. The solid line is a second-order polynomial fit to the absorption coefficient between 0.05 and 0.55 THz. The horizontal dotted lines indicate the sample thicknesses of 1, 10, 20, and 50 mm, available for the measurements.

at 1.63, lower than the previously published value at 1.67 [24]. The absorption coefficient increases quadratically, also in accordance with [24]. Note that small shifts in the refractive indices of plastics at T-ray frequencies are known to be caused by slight hygroscopicity [11] and differences in the manufacturing process.

The optimum thickness for PVC, which supposedly yields the lowest variance in the measured optical constants, is determined from the absorption coefficient using the proposed model in Eq. (11). However, the measured absorption coefficient contains error from noise, water-vapor absorption, and Fabry-Pérot fringes. By assuming that the absorption coefficient is well described by a parametric function, the measured coefficient is initially smoothed by a second-

#94045 - $15.00 USD Received 20 Mar 2008; revised 30 Apr 2008; accepted 1 May 2008; published 6 May 2008

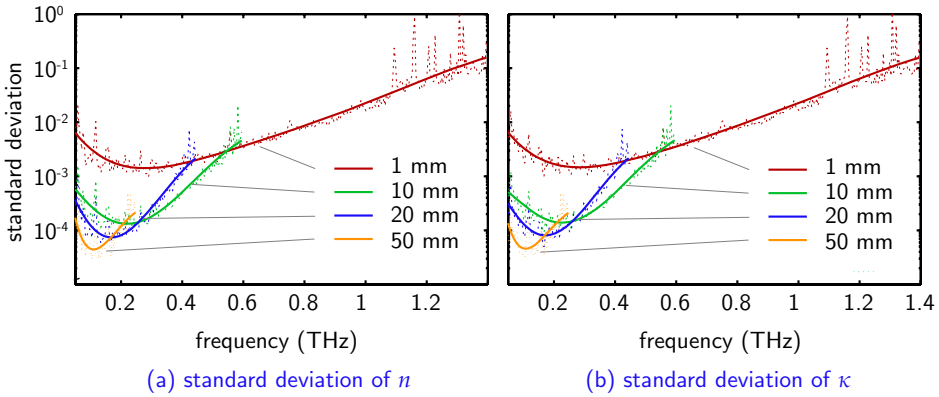

Fig. 5. Standard deviations in the optical constants of PVC. Each standard deviation is determined from ten reference and ten sample signals. The dotted lines represent the raw profiles obtained from Eq. (3), whereas the solid lines are from an analytical function, $\exp(a_1x^6+a_2x^5+\ldots+a_6x+a_7)$, fitted to the dotted lines. The missing part of the profiles in the high frequency range corresponds to the low SNR portion of the measured spectra.

order polynomial, which also enables extrapolation of the coefficient towards a higher frequency range. Figure 4 illustrates the optimum thickness determined directly from the measured coefficient and from the fitting model. It can be seen that at frequencies around 1.0 THz, a sample thickness of 1 mm would provide the lowest variance of the optical constants. In addition, at low frequencies the optimum thickness increases by around one order of magnitude.

Figure 5 shows the standard deviations of the optical constants for the four PVC samples, in terms of the unprocessed scatter plots and the fitting parametric curves. It is evident that at 0.05-0.2 THz, the 50-mm-thick sample provides the lowest standard deviation among the four samples; at 0.2-0.25 THz, the 20-mm-thick sample; at 0.25-0.6 THz, the 10-mm-thick sample; and above 0.6 THz, the 1-mm-thick sample. This optimum relation is in perfect agreement with the prediction in Fig. 4, which is derived using the proposed optimal-thickness model. The improvement in measurement accuracy can be observed, for example, by comparing the standard deviations of the 1-mm-thick and 50-mm-thick sample. At around 0.1 THz the standard deviation for the thicker sample is $\approx 4\times10^{-5}$, and that for the thinner sample is $\approx 2\times10^{-3}$, or the improvement of the standard deviation is by almost two orders of magnitude.

4.2. High-density polyethylene: HDPE

The material used in this experiment is a high-density polyethylene (HDPE), supplied as a long cylindrical rod with a diameter of 50 mm. The rod is sliced into six samples, with the thickness of 1 (1.006), 10 (9.809), 20 (19.943), 50 (50.040), 100 (100.697), and 200 (201.294) mm. THz-TDS measurements are made in the axial direction of the samples with ten scans for each sample. The interval between each scan is 45 sec.

Figure 6 shows the optical properties of HDPE, extracted from the 50-mm sample. The phase at low frequencies is extrapolated from that between 0.05 and 1 THz. Obviously, the refractive index is constant at 1.512 over the frequency range, and the absorption coefficient is nearly zero. The estimated refractive index is slightly lower than previously published values at 1.53 [22, 24], but the extinction coefficient is comparable to that in [24].

Further analysis shows that the optimum thickness of HDPE determined using Eq. (11) is higher than 20 mm for the frequency below 2 THz, as shown in Fig. 7. These sample thicknesses, although relatively thick, are expected to provide the lowest uncertainty in the measure-

#94045 - $15.00 USD Received 20 Mar 2008; revised 30 Apr 2008; accepted 1 May 2008; published 6 May 2008

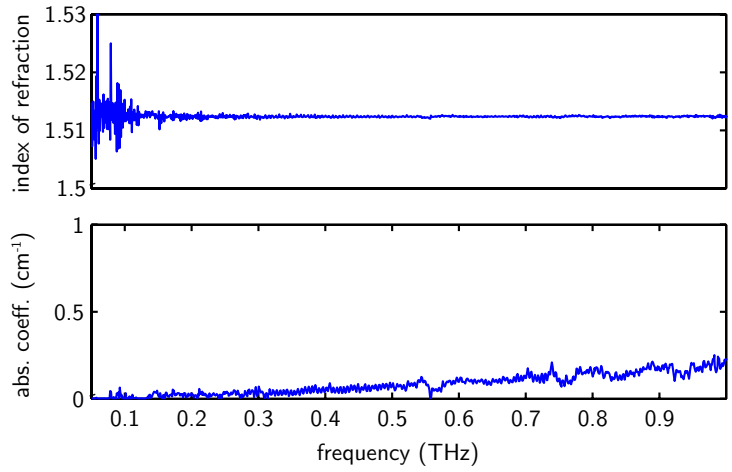

Fig. 6. Optical constants of HDPE. The constants are calculated from the average signal probing the 50-mm-thick sample. The noise in the refractive index at low frequencies is due to the low SNR of the probing signal.

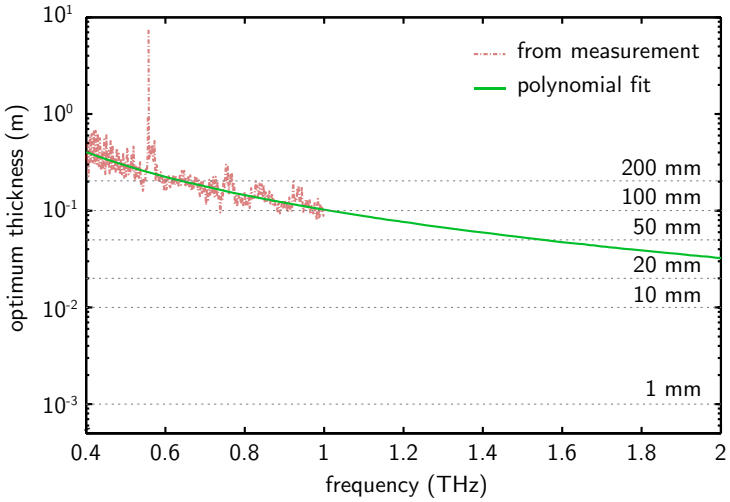

Fig. 7. Optimum thickness for HDPE. The optimum thickness is determined from the measured absorption coefficient. The solid line is a second-order polynomial fit to the absorption coefficient between 0.05 and 1 THz. The horizontal dotted lines indicate the sample thicknesses of 1, 10, 20, 50, 100, and 200 mm, available for the measurements.

#94045 - $15.00 USD Received 20 Mar 2008; revised 30 Apr 2008; accepted 1 May 2008; published 6 May 2008

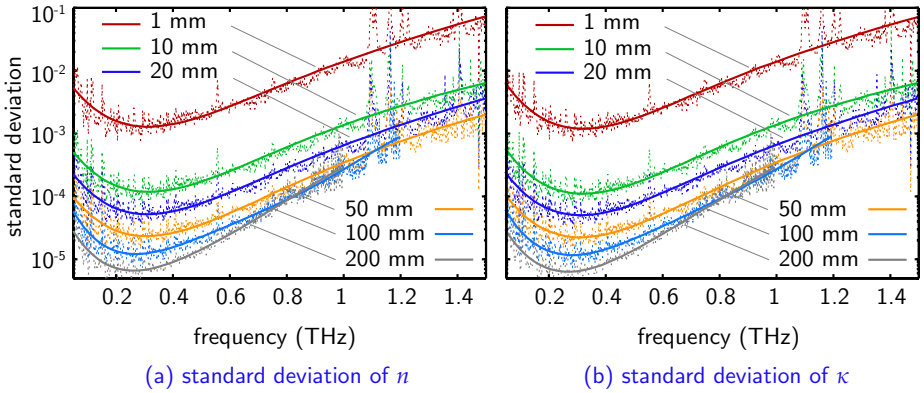

Fig. 8. Standard deviations in the optical constants of HDPE. Each standard deviation is determined from ten reference and ten sample signals. The dotted lines represent the raw profiles obtained from Eq. (3), whereas the solid lines are from an analytical function, $\exp(a_1x^5+a_2x^4+\ldots+a_5x+a_6)$, fitted to the dotted lines. The missing part of the profiles in the high frequency range corresponds to the low SNR portion of the measured spectra.

ment of the optical constants. It is evident that the prepared thicknesses of 1, 10, and 20 mm are suboptimal at all frequencies of interest, and, thus, measurement at these thicknesses is vulnerable to high uncertainty. Besides, the sample thicknesses of 50, 100, and 200 mm are the best for measurement at 1.6, 1.0, and 0.6 THz, respectively.

Figure 8 confirms the predicted optimum thickness for HDPE. By measuring the samples at various thicknesses, the standard deviations of the measured optical constants can be compared. The sample thickness of 1 mm results in the highest standard deviation for the given samples, and increase of the thickness reduces the deviation proportionally. The 50 mm sample leads to the lowest standard deviation around 1.1 to 1.5 THz; the 100 mm sample, around 0.8 to 1.1 THz; and the 200 mm sample, below 0.8 THz. The results are in excellent agreement with the optimum thickness predicted earlier in Fig. 7. In addition, between 0.05 and 1.0 THz, the standard deviation for the 200-mm-thick sample is better than that for the 1-mm-thick sample by two orders of magnitude.

4.3. Lactose

The sample materials used so far in Sections 4.1 and 4.2 have rather featureless spectra. In contrast, for a more general case, polycrystalline α-lactose monohydrate is selected for this experiment, because it has a distinctive absorption spectrum due to intermolecular resonance modes at lower T-ray frequencies. The sample pellets of lactose with different thicknesses are prepared from lactose powder ground together with ultra-high molecular weight (u.h.m.w.) polyethylene powder in the mass ratio of 1:3. The mixture powder is pressed at 10 tonnes by a hydraulic press to produce six pellets with the diameter of 13 mm and the thicknesses from 0.4 (0.440), 0.8 (0.876), 1.6 (1.658), 2.4 (2.385), 3.2 (3.196), to 4.0 (4.014) mm, all with optical-graded surfaces. The pellets are measured with a focused T-ray beam. Eight scans are recorded for each pellet, and another eight for the reference. For this experiment, the ambient measurement atmosphere is purged with nitrogen to reduce the effects of water vapor absorption. It is worth noting that the measured results are not for pure α-lactose monohydrate, but rather a α-lactose monohydrate/u.h.m.w. PE mixture. However, for conciseness, this mixture is referred to as the *lactose mix* hereafter.

The optical constants for the lactose mix, shown in Fig. 9, are determined from the 1.6-mm

#94045 - $15.00 USD Received 20 Mar 2008; revised 30 Apr 2008; accepted 1 May 2008; published 6 May 2008

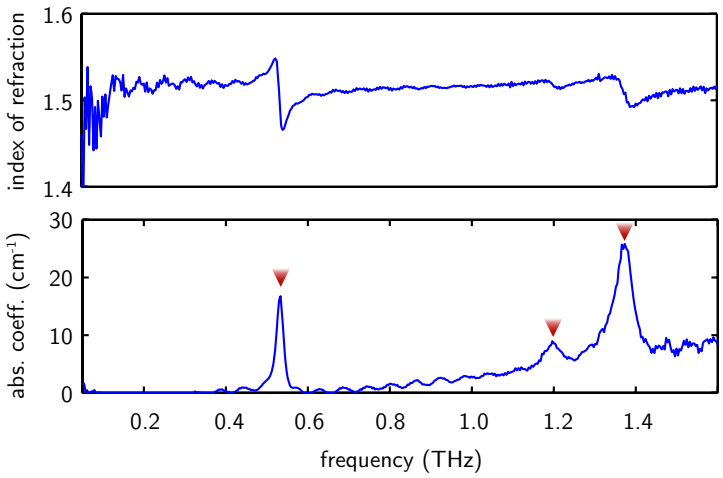

Fig. 9. Optical constants of the lactose mix. The constants are calculated from the average signal probing the 1.6-mm sample. The absorption peaks are pronounced at 0.53, 1.2, and 1.37 THz, as indicated by the arrowheads, before the spectrum is overwhelmed by noise beyond 1.6 THz.

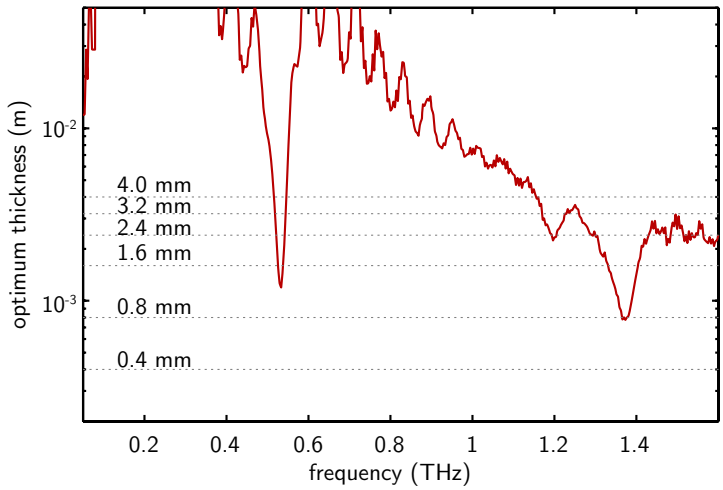

Fig. 10. Optimum thickness for the lactose mix. The optimum thickness is determined from the measured absorption coefficient. The horizontal dotted lines indicate the sample thicknesses of 0.4, 0.8, 1.6, 2.4, 3.2, to 4.0 mm, available for the measurements.

sample. The phase data at the frequencies lower than 0.05 THz are extrapolated from the data from 0.05 to 1.0 THz. Below 1.6 THz, the average value of the refractive index is 1.513, and the absorption coefficient is less than 30 cm^{-1}. The strong absorption peaks, clearly observable at 0.53, 1.2, and 1.37 THz, reproduce the results published in [25].

The optimum thickness for the lactose mix, plotted in Fig. 10, is determined from the measured absorption coefficient using the developed equation. For those frequencies below 1.2 THz, which contain no absorption peak, the optimum thickness is higher than 4.0 mm. The available thicknesses of the sample are likely to provide the lowest measurement uncertainty of the optical constants around the vicinities of absorption peaks. More specifically, the 1.6-mm sample

#94045 - $15.00 USD Received 20 Mar 2008; revised 30 Apr 2008; accepted 1 May 2008; published 6 May 2008

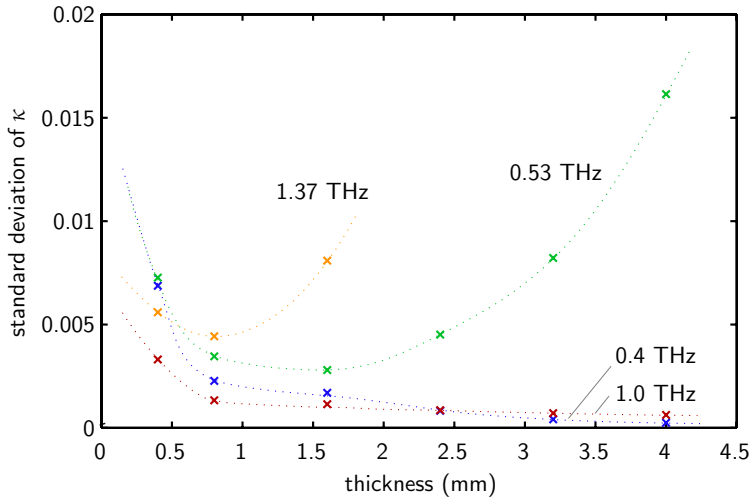

Fig. 11. Standard deviation in the extinction coefficient of the lactose mix. The values at each thickness, indicated by the crosses, are determined from eight reference and eight sample signals, using the Monte Carlo method. The frequencies 0.53 and 1.37 THz correspond to the two first significant absorption peaks of the lactose spectrum. The missing part of the 1.37-THz profile is due to the low SNR portion of the measured spectra. The standard deviation in the index of refraction has a comparable value, and hence is not shown here. The dotted lines are fitted to the measurements only for visualization.

should give the lowest uncertainty for the absorption peak at 0.53 THz, and the 0.8-mm sample gives the lowest uncertainty for the peak at 1.37 THz.

To confirm the prediction of the optimum thickness, the standard deviation in the optical constants is determined, via the Monte Carlo method, from the repeated measurements. As shown in Fig. 11, the values of the standard deviation at each interesting frequency are plotted against the thickness for clarity. Two frequencies at 0.53 and 1.37 THz are the locations of the absorption peaks of lactose, whilst another two frequencies at 0.4 and 1.0 THz are the locations of the baseline away from the peaks. It is clear from Fig. 11 that at 0.53 and 1.37 THz, the sample thicknesses of 1.6 and 0.8 mm provide the lowest standard deviation in measurement, respectively. At the frequencies of baseline, i.e. 0.4 and 1.0 THz, no optimum thickness is found in the thickness range between 0.4 and 4 mm, and the standard deviation profiles become lower towards a thicker sample thickness. The results in Fig. 11 hence justify the prediction of the optimum thickness in Fig. 10.

5. Usage of the model

The proposed model for optimum thickness is frequency-dependent, and thus it can determine the thickness for materials with any type of absorption response, provided that the absorption coefficient is available. In practice, this absorption coefficient can be measured from a preliminary sample or obtained from a published value.

When selecting the optimum thickness, two options are available: (i) have the widest measurement bandwidth, or (ii) have the lowest uncertainty at a particular frequency. If the widest bandwidth is required, the maximum absorption value within the reliable frequency range of the system should be used in determination of the optimum thickness. This results in a thinner sample thickness thus retaining the bandwidth of the system and avoids dynamic range limited distortion, while providing a reasonably low uncertainty in the measurement. There is

#94045 - $15.00 USD Received 20 Mar 2008; revised 30 Apr 2008; accepted 1 May 2008; published 6 May 2008

a possibility that one might need to observe a sample's response in a narrow frequency range, with the highest precision available from the instrument, for example, in order to resolve a weak absorption peak hidden beneath the noise or to quantify the ratio of a mixture. In such cases, the optimum thickness calculated at the frequency of interest is indeed the best selection.

Despite the thickness optimality, there are some unrestricted lower and upper limits of the thickness that are worth consideration. For a very thin sample, the non-uniformities in the sample geometry and in the bulk material tend to be pronounced. Combined with the effects of the frequency-dependent spatial distribution of the T-ray beam, relocation of the sample during measurements may cause a large variation among measured signals [26]. Although the variance in the signal's amplitude encompasses these effects, the dependence of the effects on the thickness is not taken into account in the optimization. In addition, thickness measurement for a thin sample is prone to imprecision. Due to these concerns, special care must be given to the uniformity of a sample with very thin optimum thickness and to the method of thickness measurement. Concern for reflection removal may arise in the case of optimally thin samples, for which the succeeding reflections temporally overlap and inseparable. However, an iterative parameter extraction process can cope with those overlapping reflections [27, 28]. For a very thick sample, beam defocusing may cause an overestimation of the measured absorption coefficient. A collimated beam or long-focal length beam system can alleviate the effect.

6. Conclusion

Currently, for a transmission THz-TDS measurement, there is no explicit criterion for determining an appropriate thickness for a sample under measurement in the existing literature. Traditionally, the selection of the sample thickness depends wholly on the experience of an experimentalist. In many cases, the sample thickness is preferably thin, to preserve the bandwidth of the signal. This is favorable so long as the uncertainty in optical constants is properly considered. An excessively thin sample can cause significant rise in the uncertainty of the optical constants that is influenced by measurement noise.

This work offers a criterion in selecting the optimum thickness of a sample. Provided that the absorption of a sample material at a frequency of interest can be estimated or approximated, the proposed model can predict the optimum thickness, which gives the lowest uncertainty in measurement. The derivation of the criterion is carried out via minimizing the uncertainty in optical constants—in terms of the variance or standard deviation—which is affected by the variance in measured time-resolved signals.

The experiments, performed with PVC and HDPE, representing typical and low absorption materials, confirm the validity and applicability of the derived thickness criterion. By selecting an optimum thickness for a sample under measurement, significant improvement in the standard deviation of the optical constants can be observed. These examples with monotonically increasing absorption sufficiently support the model, because the model determines the optimal thickness based on the absorption value at a particular frequency, regardless of the morphology of the absorption spectrum. In addition, as a case study, another experiment is performed with polycrystalline lactose, containing strong THz modes. An excellent agreement between the theory and the experimental results is achievable. Validated by the experiments, the proposed model can be used as a rule of thumb in selecting the thickness for a sample to achieve the minimum uncertainty in measured optical constants.

Another point, in conclusion, is that our analysis may apply in principle to optical and other regimes. However, generally speaking, the T-ray experimentalist more readily has control over the thickness, whereas the optical experimentalist tends to have more control over signal power. This explains why the analysis herein becomes generally of greater interest in the T-ray domain.

#94045 - $15.00 USD Received 20 Mar 2008; revised 30 Apr 2008; accepted 1 May 2008; published 6 May 2008

Acknowledgements

The authors appreciate the technical assistance of Alban O'Brien, Benjamin S. Y. Ung, Jegathisvaran Balakrishnan, and Henry Ho. Useful discussions with Peter Siegel of Caltech/JPL Pasadena and Samuel P. Mickan of the University of Adelaide is gratefully acknowledged. This research was supported under the Australian Research Council (ARC) *Discovery Projects* funding scheme (project number DP0556112) and the Sir Ross and Sir Keith Smith Fund.

#94045 - $15.00 USD Received 20 Mar 2008; revised 30 Apr 2008; accepted 1 May 2008; published 6 May 2008